Flow Dynamics, Acoustic generation and Heat Transfer of a Rectangular Jet Impinging on a Heated Plate

Michel Matar [1, b)], Bilal EL Zohbi[2, c)], Kamel Abed-Meraim[3, d)], Bilal Taher[1, e)], Hassan Assoum[1, 3, a)] and Anas Sakout [3, f)]

[1] *Beirut Arab University, Mechanical Engineering Department, Lebanon.*
[2] *Lebanese International University, Mechanical Engineering Department, Lebanon.*
[3] *LASIE UMR CNRS 7356, La Rochelle University, La Rochelle, France.*

[a)] *Corresponding author: h.assoum@bau.edu.lb*
[b)] *m.matar@bau.edu.lb*
[c)] *Bilal.zohbi@outlook.com*
[d)] *kabedmer@univ-lr.fr*
[e] *b.taher@bau.edu.lb*
[f)] *asakout@univ-lr.fr*

Abstract. This study investigates the coupled dynamics of flow, acoustics, and heat transfer in a rectangular jet impinging on a heated plate at a single Reynolds number of 3550. The flow field was characterized using the Q-criterion and vortex line visualization, supported by Proper Orthogonal Decomposition (POD) to extract dominant energetic modes. Acoustic measurements from four microphones and velocity probe signals within the jet were analyzed in both frequency and modal domains to identify correlations between flow structures and acoustic resonance. Finally, heat transfer reliability was assessed through the Stanton number distribution obtained from infrared thermography of the plate. Results reveal that coherent vortical structures govern both the acoustic response and the spatial distribution of Stanton number. A clear link is established between dominant flow modes, acoustic frequencies, and localized heat transfer enhancement, demonstrating the robustness of the impinging jet configuration for thermal management applications.

INTRODUCTION

Impinging jets are widely employed in high-performance cooling systems such as electronic device thermal management, gas turbine blade cooling, and material processing [1]. Their cooling efficiency depends on the complex interaction between coherent vortical structures, acoustic feedback, and heat transfer mechanisms at the impingement surface [2–5]. The unsteady behavior of the shear layer, combined with the feedback loop between the jet and the impingement surface [6–11], often leads to tonal noise and oscillatory heat transfer, which can either enhance or destabilize the overall cooling performance[12–16]. Various parameters, including the Reynolds number, jet-to-plate distance, plate material and inclination, and nozzle geometry, significantly influence the flow development and heat transfer characteristics of impinging jets [17–21]. While circular jets have been extensively studied due to their geometric simplicity and well-documented behavior, non-circular jets, particularly rectangular jets, have gained increasing attention for their potential to achieve superior mixing and improved thermal performance [22–25].

In this study, an experimental investigation is conducted to analyze the flow dynamics, acoustic behavior, and thermal reliability of a rectangular jet impinging on a heated plate at a Reynolds number of 3550. Flow visualization through Q-criterion and vortex line mapping, acoustic spectral analysis, and Proper Orthogonal Decomposition (POD) are employed to reveal the resonance between acoustic frequencies, flow structures, and thermal response. Particular attention is given to identifying the correlation between dominant frequencies and the evolution of coherent vortices that govern heat transfer modulation.

METHODOLOGY

Experimental Setup

A rectangular nozzle jet of aspect ratio 19 was directed perpendicularly toward a heated flat plate at a nozzle-to-plate distance L/H = 4 representative of practical cooling systems, as shown in FIGURE 1. The jet Reynolds number was fixed at Re=3550, based on hydraulic diameter and bulk velocity. Air was used as the working fluid. The setup starts with a control box (1) containing a frequency chopper that adjusts flow velocity, reaching up to 33 m/s, the bulk jet velocity of the nozzle is 5.5 m/s. Air is supplied by an external compressor (2), which isolates vibration noise from the test area. The flow passes through a 1 m³ damping chamber (3) with three metal grids to reduce acoustic pressure and turbulence, then moves into a 1250 mm conditioning duct (4) of 190 × 90 mm cross-section containing honeycombs for flow straightening. The air exits through a rectangular nozzle (5) of 190 × 10 mm, impinging on a 250 × 250 × 4 mm aluminum plate (6) that has a 45° slotted beveled opening (7) aligned with the jet. The test room temperature is kept between 18–20 °C using conditioned air from an adjacent controlled space.

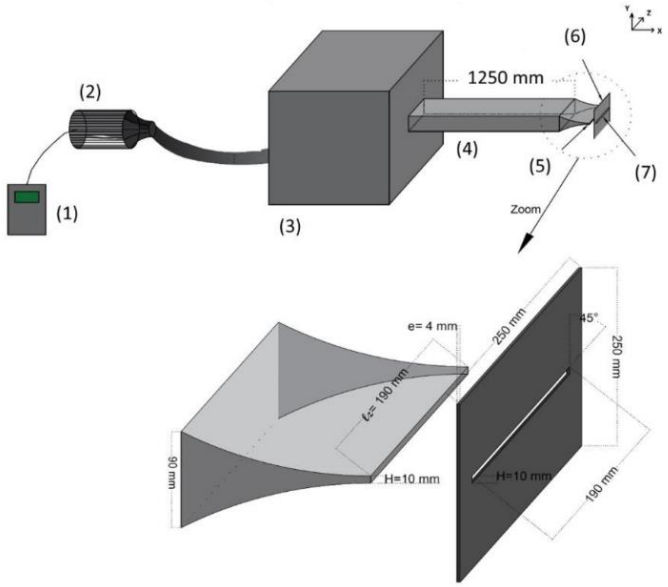

FIGURE 1. Schematic configuration (1) frequency chopper (2) compressor (3) damping volume (4) duct (5) rectangular nozzle (6) plate (7) slot.

FLOW MEASUREMENTS

Time-resolved Particle Image Velocimetry (PIV) was performed in the mid-plane of the jet to capture velocity fields. The flow was seeded with olive oil droplets (0.1–0.2 μm) produced by an oil–air atomizer using a Laskin nozzle. Illumination came from a Litron Nd:YLF LDY 304-PIV laser with dual heads, emitting 30 mJ per pulse at 527 nm and up to 1 kHz. The laser sheet thickness was adjustable, down to 0.5 mm in the measurement zone for high spatial precision. Flow images were recorded using a Phantom V711 high-speed CMOS camera, offering 1200 × 800-pixel resolution and up to 7,400 Hz at full frame. The velocity measurement uncertainty was estimated at ±2.13% of the jet exit velocity for Re = 3550.

Acoustics

Acoustic signals were measured using Brüel & Kjær Type 4189 free-field microphones (20 Hz–20 kHz). Microphones were placed around the test section to capture overall and local sound levels. Data were recorded with an NI PXIe-4496 analyzer (24-bit, 204.8 kHz/channel) and monitored in LabVIEW.

Thermal

Two infrared (IR) cameras of type Xenics Gobi-640-GigE (640 × 480 uncooled microbolometer sensors) was employed to measure wall temperature distribution.

Data Processing

Proper Orthogonal Decomposition (POD)

POD was employed on the PIV data to extract the main energetic structures of the flow. Using Singular Value Decomposition (SVD), the velocity field was expressed as

$$X = U\,\Sigma\,V^T \tag{1}$$

where U denote spatial POD modes, V temporal coefficients, and Σ the singular values. The relative energy of each mode was given by

$$E_i = \frac{\sigma_i^2}{\Sigma_j \sigma_j^2} \tag{2}$$

Where σ_i is the i-th singular value. This analysis highlights the coherent flow patterns responsible for momentum and heat transfer [26].

Stanton Number

Average heat transfer coefficients were calculated and expressed in terms of the Stanton number:

$$s_t = \frac{H}{\rho c_p U_{\text{out}}} \tag{3}$$

Where H is the convective heat transfer coefficient, ρ is the air density, U_{out} the bulk jet velocity, and c_p the specific heat capacity. The Stanton number was used to normalize the convective heat transfer coefficient and enable direct comparison of thermal performance under different flow conditions. This dimensionless form represents the efficiency of convective energy exchange between the jet and the heated surface. Its spatial distribution provides insight into the influence of coherent vortices and acoustic resonance on local cooling effectiveness, while the average value quantifies the overall thermal reliability of the impinging jet [27]

FLOW DYNAMICS

The Q-criterion was applied to visualize coherent vortical structures and analyze their evolution under different flow conditions. At Re = 3550, the main vortex changed its orientation upon striking the plate, while smaller secondary vortices developed near the surface (FIGURE 2A). This behavior agrees with previous research showing that the nozzle-to-plate spacing plays a key role in shaping vortex organization and turbulence intensity in impinging jets [28]. At this Reynolds number, vortices formed symmetrically and maintained their structure as they moved toward the slotted plate. Upon impact, two main interactions were observed: wall-following vortices that spread along the surface and propagated laterally within the region between y = 5 mm and y = 16 mm, and slot-penetrating vortices, where parts of the structures passed directly through the slot. These two mechanisms alternated periodically, producing a synchronized and repeating pattern of vortex–wall interaction. As shown in FIGURE 2B, two distinct vortex trajectories appeared between the nozzle and the plate, with secondary vortex formation becoming more evident around y = 22 mm from the jet centerline.

The POD analysis focused on the first few modes to reveal the main flow dynamics and dominant frequencies. The first eight modes (**Error! Reference source not found.**) capture the key coherent structures of the impinging jet. The first mode, accounting for 10.60% of the total energy, represents the main large-scale vortex or the strongest instability in the flow. Modes 1–4, which together contain 24.15% of the total energy, show large organized structures on both sides of the jet, following a trajectory where the vortices strike the slotted plate and then pass through it. Modes 5 and 6, contributing 6.98% of the energy, display smaller vortical structures that deform upon contact with the plate and spread laterally along the surface, indicating secondary vortex motion.

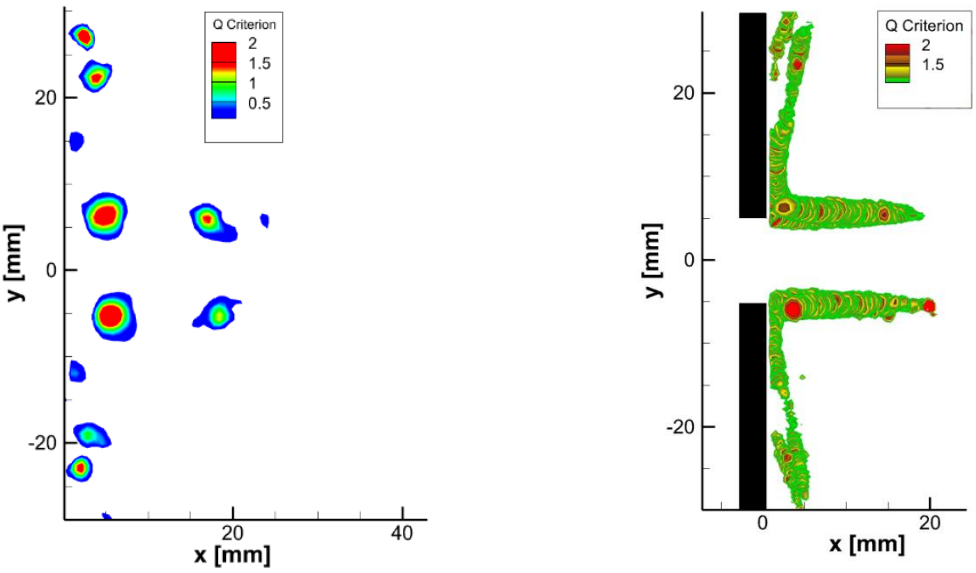

(a) (b)

FIGURE 2. (a) The Q criterion representation of the flow at T0 = 0. (b) The line vortex representation of the flow.

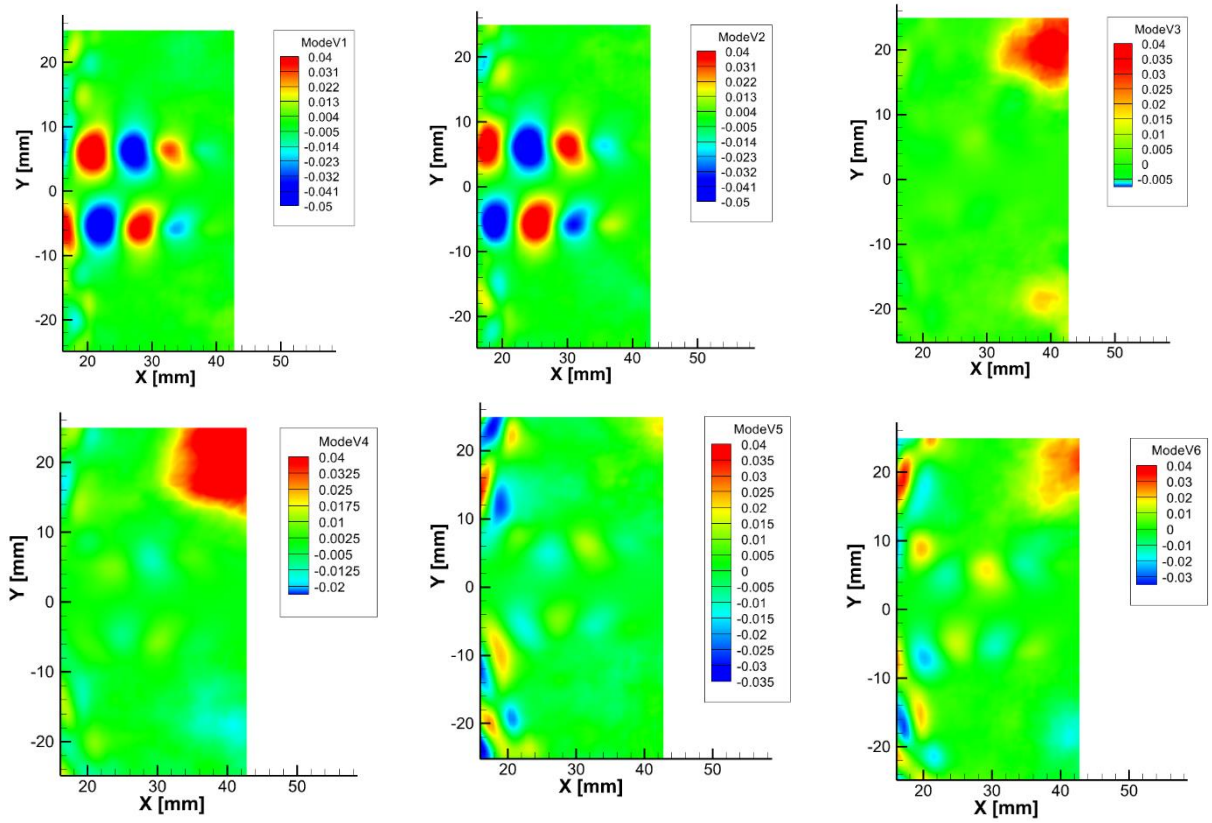

FIGURE 3. The first six POD mode.

AEROACOUSTIC ANALYSIS

Impinging jets typically generate tonal noise, which becomes stronger when the jet interacts with a slotted plate, as in this study. The microphone spectra show two main peaks at F1 = 101.3 Hz and its harmonic F2 = 202.5 Hz, along with weaker ones at F3 = 51.87 Hz (F1/2) and F4 = 303.83 Hz (3F1). The dominant frequencies F1 and F2 arise from self-sustained acoustic feedback and are linked to Kelvin–Helmholtz vortices in the jet shear layer.

FIGURE 4 displays the four points selected from the flow field. At V1, two dominant frequencies appear: F1 = 105 Hz and F2 = 202.5 Hz, with F2 having the stronger amplitude. At V2, V3, and V4, the same frequencies are detected, but F1 becomes dominant while F2 weakens. Minor peaks at F3 = 52.5 Hz, and F4 = 307.5 Hz have negligible impact. These results indicate that F1 corresponds to a symmetric vortex moving toward the plate, whereas F2 relates to another symmetric structure propagating through the slot.

The temporal spectra of the POD modes reveal two main frequency components governing the flow behavior. Modes 1, 2, and 3 are primarily driven by the higher frequency F2=202.5 Hz, with a secondary, weaker peak at $F1$ =105 Hz. In contrast, Modes 4, 5, and 6 exhibit a reversal, where F1 = 105 Hz dominates and F2=202.5 Hz appears with lower intensity. Modes 5 and 6 also contain low-amplitude energy spread over multiple frequencies. This pattern supports the flow dynamics interpretation: Modes 1–4 are linked to the main vortex motion between the nozzle and the plate, while Modes 5 and 6 correspond to the flow after impingement and the generation of secondary vortices near the slotted wall. These findings establish a strong flow–acoustic coupling: coherent vortices amplify pressure fluctuations, while acoustic feedback reinforces flow instabilities, creating a self-sustained resonance cycle.

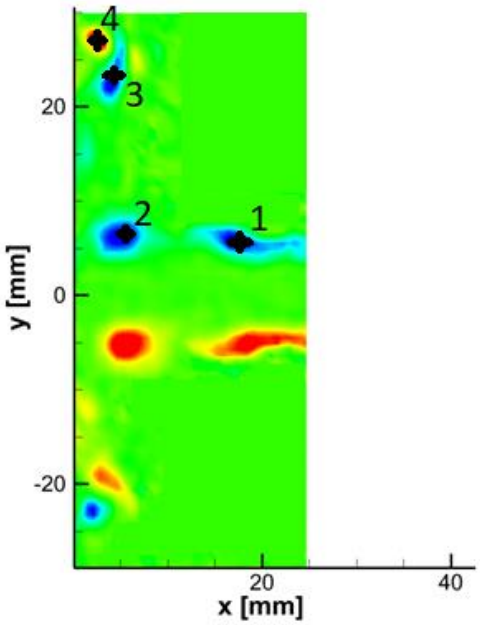

FIGURE 4. vorticity field showing the 4 locations V1, V2, V3 and V4.

HEAT TRANSFER

FIGURE 5a illustrates the interaction between the vortical structures and the thermal field near the heated wall. The line vortex visualization reveals the trajectory of the primary vortex, which sweeps along the surface from approximately Y = 5 mm to Y = 16 mm. This motion enhances convective mixing and promotes localized cooling within the impingement zone. Downstream, a secondary vortex emerges near Y ≈ 22 mm, indicating the onset of vortex pairing and partial detachment from the wall. The birth of this secondary structure corresponds to a local reorganization of the near-wall flow, which influences both the momentum and heat transport characteristics.

FIGURE 5b complements these observations by presenting the mean Stanton number (St) distribution along the Y-axis. Two distinct peaks are evident: the first, located between Y ≈ 6–16 mm; the second, around Y ≈ 22 mm, coincides with the formation of the secondary vortex before flow separation occurs, aligns with the impingement of the primary vortex shown in FIGURE 5a. The spatial correspondence between these features highlights the strong coupling between the unsteady flow dynamics and wall heat transfer behaviour.

The St variation also exhibits a mild oscillatory trend, reflecting the influence of periodic flow excitation. The enhancement regions correlate with dominant acoustic frequencies (F_1 and F_2), confirming that the resonance between the jet's hydrodynamic structures and the acoustic field governs the distribution of thermal loads on the surface. This coupled mechanism ensures a stable yet spatially modulated heat transfer pattern, emphasizing the key role of coherent vortex impingement in dictating local convective efficiency.

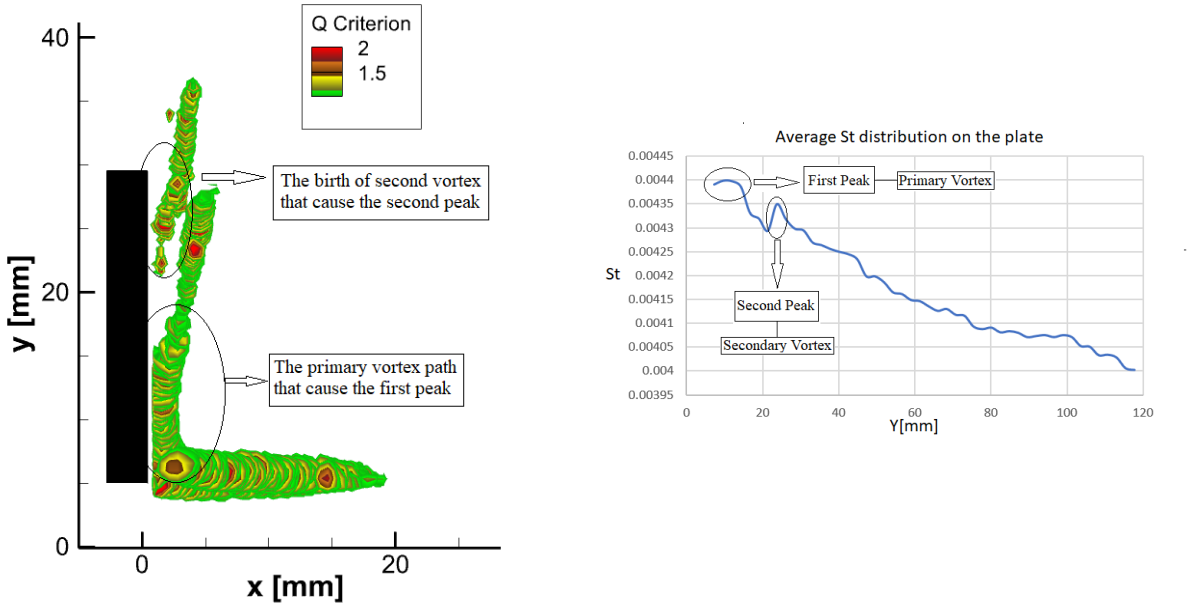

(a) (b)

FIGURE 5. (a) Vortical structures (b) Average St distribution on the plate.

CONCLUSION

An experimental investigation was carried out to analyze the flow dynamics, acoustic behavior, and thermal reliability of a rectangular jet impinging on a heated plate at Re = 3550. The study combined flow field visualization through Q-criterion and vortex lines, acoustic spectral analysis, and POD decomposition to explore the coupled flow–acoustic–thermal interactions governing the system.

The acoustic spectra revealed two dominant frequencies, F_1 = 105 Hz and F_2 = 202.5 Hz, corresponding to the fundamental and its first harmonic. These frequencies were also detected in the flow field and POD modes, confirming a resonance phenomenon between the acoustic feedback loop and the shear-layer instabilities. POD results showed that modes 1–3 were dominated by F_2, while modes 4–6 were primarily influenced by F_1, indicating strong synchronization between coherent structures and acoustic oscillations.

Thermally, the Stanton number (St) distribution exhibited a wave-like pattern, with maximum heat transfer at the jet stagnation point and a gradual decay toward the plate edges. The highest St values were found near the impingement of primary vortices, while a secondary peak appeared in correspondence with the formation of a second vortex structure, also associated with the identified acoustic frequencies. This agreement between flow structures, thermal response, and spectral content confirms that the flow–acoustic coupling directly governs the heat transfer modulation.

Future studies could explore the effect of varying the Reynolds number, jet-to-plate spacing, or slot geometry to further assess the influence of resonance on thermal performance. Implementing active flow control methods, such as piezoelectric excitation or fluidic diodes, may help regulate the acoustic feedback and enhance heat transfer efficiency. Additionally, coupling synchronized PIV, acoustic, and infrared thermography measurements could provide deeper insight into the temporal evolution and phase relationship among flow structures, acoustic modes, and thermal fluctuations.

ACKNOWLEDGMENTS

The authors wish to thank FEDER, the 'Region of Nouvelle Aquitaine' for the financial support of this research.

REFERENCES

1. Michel Matar, H. H. A., Mohammad El Hassan, Nikolay Bukharin, Anas Sakout, Ali Hammoud. Heat Transfer Characteristics of Passive, Active, and Hybrid Impinging Jets: A Review. *International Journal of Technology* **16**, 46–71 (2025).
2. Assoum, H. H., Hassan, M. E., Abed-Meraïm, K., Martinuzzi, R. & Sakout, A. Experimental analysis of the aero-acoustic coupling in a plane impinging jet on a slotted plate. *Fluid Dynamics Research* **45**, 045503 (2013).
3. Assoum, H. H., Hassan, M. E., Abed-Meraim, K. & Sakout, A. The vortex dynamics and the self sustained tones in a plane jet impinging on a slotted plate. *European Journal of Mechanics - B/Fluids* **48**, 231–235 (2014).
4. Assoum, H. H. *et al.* Experimental investigation the turbulent kinetic energy and the acoustic field in a rectangular jet impinging a slotted plate. *Energy Procedia* **139**, 398–403 (2017).
5. Mrach, T. *et al.* Experimental study of the thermal effect on the acoustic field generated by a jet impinging on a slotted heated plate. *Energy Reports* **6**, 497–501 (2020).
6. Assoum, H. H. *et al.* Turbulent Kinetic Energy and self-sustaining tones in an impinging jet using High Speed 3D Tomographic-PIV. *Energy Rep.* **6**, 802–806 (2020).
7. Assoum, H. *et al.* Correlation between the acoustic field and the transverse velocity in a plane impinging jet in the presence of self-sustaining tones. *Energy Procedia* **139**, 391–397 (2017).
8. Assoum, H. *et al.* Spatio-Temporal Changes in the Turbulent Kinetic Energy of a Rectangular Jet Impinging on a Slotted Plate Analyzed with High Speed 3D Tomographic-Particle Image Velocimetry. *IJHT* **37**, 1071–1079 (2019).
9. Assoum, H. H. *et al.* Tomographic Particle Image Velocimetry and Dynamic Mode Decomposition (DMD) in a Rectangular Impinging Jet: Vortex Dynamics and Acoustic Generation. *Fluids* **6**, 429 (2021).
10. El Zohbi, B. *et al.* Experimental investigation of the Aero-Acoustics of a rectangular jet impinging a slotted plate for different flow regimes. *Alexandria Engineering Journal* **87**, 404–416 (2024).
11. Assoum, H. H. *et al.* Control of a rectangular impinging jet: Experimental investigation of the flow dynamics and the acoustic field. *Alexandria Engineering Journal* **79**, 354–365 (2023).
12. Xu, F., Patterson, J. C. & Lei, C. Transition to a periodic flow induced by a thin fin on the sidewall of a differentially heated cavity. *International Journal of Heat and Mass Transfer* **52**, 620–628 (2009).
13. Geng, L., Zheng, C. & Zhou, J. Heat transfer characteristics of impinging jets: The influence of unsteadiness with different waveforms. *International Communications in Heat and Mass Transfer* **66**, 105–113 (2015).
14. Zhao, Y., Zhao, P., Liu, Y., Xu, Y. & Torres, J. F. On the selection of perturbations for thermal boundary layer control. *Physics of Fluids* **31**, 104102 (2019).
15. Zhao, Y., Lei, C. & Patterson, J. C. PIV measurements of the K-type transition in natural convection boundary layers. *Experimental Thermal and Fluid Science* **101**, 62–75 (2019).
16. Zhao, Y., Lei, C. & Patterson, J. C. Natural transition in natural convection boundary layers. *International Communications in Heat and Mass Transfer* **76**, 366–375 (2016).
17. Matar et al. (2024). Turbulent Flow and Heat Transfer Characteristics of Resonant Impinging Jets - State of the Art Review. *International Journal of Heat and Technology, Vol. 42, No. 5, pp. 1525-1533. https://doi.org/10.18280/ijht.420505*.
18. Jenkins, R., Lupoi, R., Kempers, R. & Robinson, A. J. Heat transfer performance of boiling jet array impingement on micro-grooved surfaces. *Experimental Thermal and Fluid Science* **80**, 293–304 (2017).
19. Rakhsha, S., Zargarabadi, M. R. & Saedodin, S. The effect of nozzle geometry on the flow and heat transfer of pulsed impinging jet on the concave surface. *International Journal of Thermal Sciences* **184**, 107925 (2023).

20. He, C. & Liu, Y. Jet impingement heat transfer of a lobed nozzle: Measurements using temperature-sensitive paint and particle image velocimetry. *International Journal of Heat and Fluid Flow* **71**, 111–126 (2018).
21. Zohbi, B. E. *et al.* Investigation of the effects of the jet nozzle geometry and location on the performance of supersonic fluid ejectors. *Energy Reports* **8**, 228–233 (2022).
22. Crispo, C. M., Greco, C. S. & Cardone, G. Convective heat transfer in circular and chevron impinging synthetic jets. *International Journal of Heat and Mass Transfer* **126**, 969–979 (2018).
23. Assoum, H. H. *et al.* Control of a rectangular impinging jet: Experimental investigation of the flow dynamics and the acoustic field. *Alexandria Engineering Journal* **79**, 354–365 (2023).
24. Wang, L., Feng, L., Xu, Y., Xu, Y. & Wang, J. Experimental investigation on flow characteristics and unsteady heat transfer of noncircular impinging synthetic jets. *International Journal of Heat and Mass Transfer* **190**, 122760 (2022).
25. Trinh, X. T., Fénot, M. & Dorignac, E. The effect of nozzle geometry on local convective heat transfer to unconfined impinging air jets. *Experimental Thermal and Fluid Science* **70**, 1–16 (2016).
26. *Lumley, J.L. 1967 The Structure of Inhomogeneous Turbulent Flows, In A.M. Yaglom, & V.I. Tatarski Atmospheric Turbulence & Wave Propagation, 166–178.*
27. Wassenberg, J., Stephan, P. & Gambaryan-Roisman, T. Heat transfer during pulsating liquid jet impingement onto a vertical wall. *Heat and Mass Transfer* **57**, 617–629 (2021).
28. Assoum, Hassan H., et al. 'Experimental analysis of the aero-acoustic coupling in a plane impinging jet on a slotted plate.' Fluid Dynamics Research 45.4 (2013): 045503.